

## Estimation of Photosynthetic Photon Flux Density from 368-nm Spectral Irradiance\*

RICHARD H. GRANT

*Purdue University, West Lafayette, Indiana*

JAMES R. SLUSSER

*Colorado State University, Fort Collins, Colorado*

(Manuscript received 14 May 2003, in final form 6 October 2003)

### ABSTRACT

The estimation of photosynthetically active radiation across the earth's surface is needed to model plant productivity and future impacts of ultraviolet-B (UV-B) radiation on plant productivity. While radiation in the ultraviolet and visible wavelengths is routinely measured using broadband and multifilter rotating shadowband radiometers in the United States Department of Agriculture (USDA) UV-B Climate Monitoring Network, measurements of photosynthetically active radiation have not been made prior to 2002. Three models were developed to estimate the photosynthetic photon flux density (PPFD) from measurements of the diffuse and global spectral irradiance at 368 nm made by multifilter rotating shadowband radiometers. The models were developed from measurements made at half-hour intervals between March and November 2002 at five USDA UV-B Climate Monitoring Network locations in the United States between 34° and 43°N latitude and 77° and 112°W longitude. The model that best estimated the PPFD included global and diffuse 368-nm irradiance, solar zenith angle, sky brightness, and aerosol transmittance and had a residual error of 79  $\mu\text{mol m}^{-2} \text{s}^{-1}$  PPFD. The best two-variable model for estimating PPFD utilized measured global and diffuse 368-nm irradiance, with a root-mean-squared error of 85  $\mu\text{mol m}^{-2} \text{s}^{-1}$ . Since errors of the order of 80  $\mu\text{mol m}^{-2} \text{s}^{-1}$  represent biologically significant amounts of dry matter production in crops and the 9% model error is approximately twice that of the nominal measurement error for the PPFD sensor, PPFD measurements should be made and not modeled wherever possible.

### 1. Introduction

Changes in the spectral distribution of radiation due to global climate change can impact intensively managed and natural terrestrial ecosystems since plant growth, maturation, and productivity are heavily influenced by the quality and quantity of the radiation. Changes in stratospheric ozone and clouds influence the ultraviolet-B (UV-B; 280–320 nm) solar radiation at the earth's surface. Changes in clouds and aerosols influence longer wavelengths of solar radiation including the ultraviolet-A (UV-A; 320–400 nm) and photosynthetically active radiation (PAR; 400–700 nm) reaching the earth's surface. The relative growth rate and net carbon assimilation rate of plants depends in part on the plant-intercepted PAR [termed photosynthetic photon flux density (PPFD)] and the pathway the plant uses to assimilate the carbon. This carbon assimilation can be

inhibited and plant productivity reduced by UV-B and UV-A solar radiation (Cen and Bornman 1990; Taylor et al. 1997; Vass et al. 2002; Flint and Caldwell 2003). UV-B impacts on plant carbon assimilation are, however, influenced by the proportion of PAR to UV-B radiation reaching the plant leaf. Low PPFD levels (50–150  $\mu\text{mol m}^{-2} \text{s}^{-1}$ ) typically result in enhanced UV-B effects (Cen and Bornman 1990) while high PPFD ( $\approx 450 \mu\text{mol m}^{-2} \text{s}^{-1}$ ) appears to repair UV-B damage (Taylor et al. 1997).

The impacts of UV-B radiation on carbon assimilation in plants are not limited to plant morphology, development, and productivity. Secondary effects of UV-B radiation on terrestrial plants include changes in susceptibility to insect herbivory and pathogen infection through changes in the plant's metabolism (Caldwell et al. 2003). UV-B may ultimately affect the composition and biogeochemical cycling of terrestrial ecosystems through influencing decomposition rates and relative plant competition (Zepp et al. 2003). Consequently, biologists need to know the incident PPFD as well as UV-B and UV-A radiation to understand the UV-B and UV-A effects on plants and ecosystems.

The estimation of global PPFD from global shortwave (SW; 300–3000 nm) solar radiation measurements has

\* Purdue Agricultural Research Station Manuscript Number 17093.

Corresponding author address: Dr. Richard H. Grant, Purdue University, 1150 Lilly Hall of Life Sciences, West Lafayette, IN 47907-1150.

E-mail: rgrant@purdue.edu

been studied by many researchers (Blackburn and Proctor 1983; Gueymard 1989a,b; Olsen and Skartveit 1993; Alados et al. 1996; González and Calbó 2002). The partitioning of clear-sky solar radiation into direct beam and diffuse sky radiation in the wavelengths above those affected by column ozone ( $>320$  nm) depends on the surface albedo as well as the composition, distribution, and amount of aerosols present. González and Calbó (2002) found the ratio of global PAR/global SW was strongly affected by column water vapor and airmass number. Although acknowledged as important in the ratio, they did not include the effects of aerosols in their model. The combined effects of aerosol composition, distribution, and amount is represented by the aerosol optical depth (AOD). AOD has been used by Gueymard (1989a) and others to model PPFD based on scattering theory. Using modeled data for global SW and PAR, Gueymard (1989b) estimated that the global PAR irradiances under clear skies could be estimated given the global SW and the airmass number.

Modeling the PPFD under variable partly cloudy skies typically results in poorer accuracies than under clear skies due to the inhomogeneity of clouds and cloud properties. The estimation of global PAR or PPFD from that of SW relies on the similarity of the atmospheric scattering and absorption processes for the two wave bands. Under cloudy skies the global PAR/global SW ratio varies with cloud cover (McCree 1966; Blackburn and Proctor 1983; Rao 1984). This variation is in part due to the changes in diffuse fraction with solar zenith angle or airmass number. For daily PPFD exposures, the global PAR/global SW ratio is relatively insensitive to cloud cover (Blackburn and Proctor 1983; Rao 1984) such that over the course of a half-year a single value can account for 99% of the variability in PAR (Blackburn and Proctor 1983). Such a single ratio has been used widely to estimate global PPFD from global SW (McCree 1966; Howell et al. 1983; Rao 1984; Karalis 1989; Papaioannou et al. 1993).

A second approach to modeling the PPFD is to separately model the direct beam and diffuse sky radiation components of the global irradiance. Many models have simulated the two components separately basing the diffuse component model on semiempirical relationships (Spitters et al. 1986; Gueymard et al. 1989b). This semiempirical modeling, however, introduces additional sources of error since the fraction of diffuse radiation and direct beam radiation varies with cloud cover and wavelength band. Spitters et al. (1986) determined that the diffuse fraction of the PPFD was 1.4 times that of the diffuse fraction of SW, while Karalis (1989) found that the direct beam PPFD to direct beam SW varied from 0.2 to 0.4 depending on cloud conditions. Studies have shown less difference in the diffuse fractions between the PAR and UV wave bands, with the partitioning of solar radiation largely determined by the scattering of the cloud particles with little wavelength dependency (Scheirer and Macke 2001) resulting in sim-

ilar partitioning for a given cloud fraction (Grant and Gao 2003). Analysis of the results of Jacovidis et al. (1997) however showed the irradiance ratio of PAR to UV (defined as 300–400 nm) varied more in the diffuse component [13% coefficient of variation (CV)] than for the global irradiance (7% CV) even though the UV to PAR ratio of the global irradiances was twice that of the diffuse-only component.

An alternative to modeling the two components of the PPFD from existing global irradiance measurements is the modeling of the global PPFD from measurements made of the direct and diffuse radiation at another wavelength. This approach has the advantage of reducing the error associated with variable cloud cover. Models by Alados et al. (1996), Alados and Alados-Arboledas (1999a,b), and Jacovidis et al. (2003) have estimated diffuse and direct beam PPFD from diffuse and direct beam SW.

The United States Department of Agriculture (USDA) UV-B Climate Monitoring Network (Bigelow et al. 1998) needs to be able to retrospectively estimate PPFD at locations in the network based on previously measured irradiances made by either the visible multifilter rotating shadowband radiometer (VIS-MFRSR; Yankee Systems, Inc.) or the UV multifilter rotating shadowband radiometer (UV-MFRSR; Yankee Systems, Inc.). Since rotating shadowband radiometers used throughout the network provide both the global irradiance and the diffuse-only irradiance (Harrison et al. 1994), measurements made by this class of radiometers provide a means to estimating PPFD. Ideally, the PPFD would be estimated from the narrow band spectral irradiance measurements made by the VIS-MFRSR since they span the PAR wavelength range. Unfortunately, the interference filters used in the VIS-MFRSR instrument were not wave band-stable over time and as a result the instrument did not hold its calibration for an extended period of time. Consequently, PPFD needed to be estimated using the more-stable UV-MFRSR (Bigelow and Slusser 2000). The UV-MFRSR has channels centered on nominal center wavelengths of 300, 305, 311, 317, 325, 332, and 368 nm. Of these channels, the 368-nm channel, with a nominal bandwidth of 2 nm, is closest to the PAR wave band.

The objective of this project was to determine whether the measured PPFD could be modeled using the measurements from the UV-MFRSR 368-nm channel with sufficient accuracy for plant-effects researchers to determine UV-B impacts. As previously stated, estimation of PPFD based on 368-nm irradiance depends on the similarity of the aerosol and molecular scattering and absorption between the two wave bands under clear and cloudy skies. Although aerosols scatter and absorb with differing efficiencies across the wavelengths of interest, the differences are very small. Jacovidis et al. (1997) found for clear skies and low pollutant levels that the change in atmospheric absorption did not vary between the PAR and the UV-B. Molecular scattering decreases

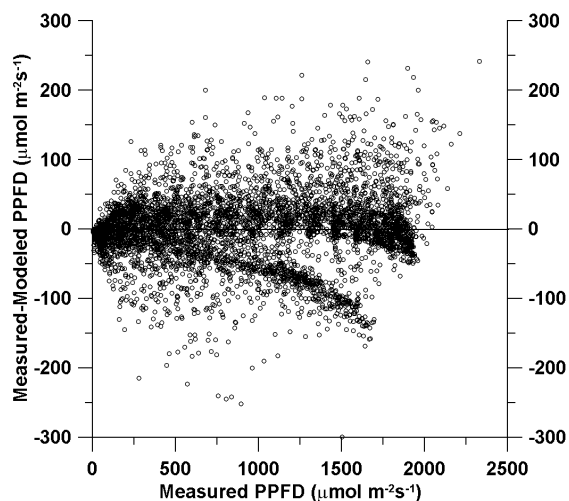


FIG. 1. Residual analysis for the UT measurement location of the model based only on global 368-nm measurements and solar zenith angle (model 1).

with increasing wavelength while molecular absorption is similar except that ozone absorbs very weakly in the PAR wave band and not at all at 368 m.

## 2. Methods

Measurements of the 368-nm global ( $R_{s,368}$ ) and diffuse irradiance ( $R_{d,368}$ ) and PPFD were made at five locations in the USDA UVB Climate Monitoring Network between March and November 2002 (Fig. 1, Table 1). All locations included in the study are in predominantly rural environments, so variation in surface albedo was assumed to be negligible among the locations. Values used in this study were 3-min averages of 20-s global and diffuse 368-nm irradiance measurements and PPFD made every 30 min. The mean PPFD at each location is indicated in Table 2.

The AOD at 368 nm was determined according to Harrison and Michalsky (1994) for all valid 3-min averages. Since AOD can only be computed for days and hours with a significant direct beam component, these calculations were not made for all days. The AOD values however were computed under both clear and partly cloudy skies and consequently include the effects of thin translucent clouds. All valid 3-min values of AOD with solar zenith angles less than  $70^\circ$  were averaged to a mean daily value and utilized in the developed models.

As a result of these restrictions not all irradiance measurements had a corresponding estimate of AOD. The mean daily AOD at the five locations over the period of study varied from a low of 0.62 at Utah to a high of 1.32 at Mississippi (Table 2).

Measurements of the PPFD were made using LiCOR 190SB sensors calibrated by the factory within a year of the measurements (Table 1). The PAR sensor has an absolute measurement error of  $\pm 5\%$  and a cosine response error of less than 5% for solar zenith angles of up to  $80^\circ$  (LiCOR, Inc. 1986). To maintain high quality values for modeling purposes, all PPFD values with solar zenith angles more than  $80^\circ$  were excluded. This reduced the sample size by 14% to 17 916 records.

Measurements of the 368-nm global and diffuse irradiance were made using UV-MFRSR instruments (Yankee Environmental Systems, Inc.) maintained with approximately yearly calibrations by the Central UVB Calibration Facility (Bigelow and Slusser 2000). Frequent checks on the calibration are made using Langley plots (Slusser et al. 2000). The calibration histories for these sensors are reported in Table 1. The UV-MFRSR sensors have a cosine response error of less than 5% up to  $76^\circ$  (Grant and Gao 2003) and are individually corrected for cosine response to an estimated error of  $\pm 1.5\%$  (Grobner et al. 1996). The cumulative sources of UV-MFRSR measurement error result in an approximately  $\pm 8\%$  error (Bigelow and Slusser 2000).

The PPFD was modeled for each individual location and for the combination of all locations using the variables  $R_{s,368}$ ,  $\Theta$ , aerosol transmittance ( $\tau$ ), 368-nm diffuse fraction ( $D_{368}$ ),  $D_{368}^2$ , and sky brightness ( $\Delta$ ). The diffuse fraction was defined as

$$D_{368} = R_{d,368}/R_{s,368}, \quad (1)$$

while the sky brightness was defined as

$$\Delta = R_{d,368}/1.58 \cos\Theta, \quad (2)$$

where  $1.58 \text{ W m}^{-2}$  ( $\pm 0.41 \text{ W m}^{-2}$ ) represents the mean value of extraterrestrial irradiance measurable by the 368 channel of the individual UV-MFRSR instruments (Table 1). The mean values of  $\Delta$  at each measurement location are indicated in Table 2. The aerosol transmittance was defined by

$$\tau = e^{-m\text{AOD}}, \quad (3)$$

where  $m$  is the airmass number.

Regressions were developed using both SAS and TA-

TABLE 1. Measurement locations and sensor histories. Number of records used in the stepwise regression analyses is indicated by "No."

Location	Lat ( $^\circ\text{N}$ )	Lon ( $^\circ\text{W}$ )	Dates of UV-MFRSR calibration	Dates of UV-MFRSR head change	Date of PPFD calibration	No.
Nunn, CO	40.8	104.8	14 Jul 2001, 21 May 2002	7 Oct 1999, 24 Aug 2002	14 Jul 1998	4756
West Lafayette, IN	40.5	87.0	14 Feb 2001, 19 Apr 2002	6 Apr 2001, 7 May 2002	6 Jun 2002	911
Starkville, MS	33.5	88.8	22 Aug 2001, 5 Nov 2002	5 Nov 2001, 21 Nov 2002	13 May 2002	3126
Geneva, NY	42.9	77.0	25 Mar 2002, 5 Mar 2002	29 Oct 1999, 25 Mar 2002	20 Mar 2002	4038
Logan, UT	41.7	111.9	22 Aug 2001, 5 Feb 2003	2 Nov 2001, 27 Mar 2003	20 Mar 2002	4559

TABLE 2. Atmospheric conditions and modeling errors for each measurement location. Model rms errors based on location-specific regression models using the same variables as the reported all-location models.

Location	Mean PPFD ( $\mu\text{mol m}^{-2} \text{s}^{-1}$ )	Mean AOD	Mean $\Delta$	Rms error ( $\mu\text{mol m}^{-2} \text{s}^{-1}$ )		
				Variables of unlimited model	Variables of model 1	Variables of model 2
Nunn, CO	956	0.84	0.23	64	72	69
W. Lafayette, IN	1016	1.07	0.28	45	52	60
Starkville, MS	877	1.32	0.23	59	66	68
Geneva, NY	825	1.27	0.24	65	71	69
Logan, UT	1024	0.62	0.22	51	62	55

BLECURVE. SAS had the advantage of being able to incorporate as many variables as desired, while TABLECURVE was able to evaluate nonlinear models but only two variates. All parameters used in the models included here had value estimates significantly different from zero at the 0.01 level. Variables included in the presented models had F statistics that were significant at the 0.15 level. Models were chosen from those developed by TABLECURVE according to the F statistic, low rmse, and no more than four terms. Model residuals were compared to the magnitude of the irradiance and solar zenith angle. The number of records used in the various models varied according to the availability of all values for a given record. The minimum number of records, where all variables described earlier were available, occurred for the stepwise SAS regressions and are reported in Table 1.

For comparisons with other studies, the conversion from PAR to PPFD assumed a quanta per joule energy of  $4.56 \mu\text{mol J}^{-1}$  (McCartney 1978).

### 3. Results and discussion

The linear correlations between measured PPFD and  $R_{s,368}$  and  $R_{d,368}$  for all locations for the period of record were 0.99 and 0.80 respectively. These are similar to the correlations between PPFD and global solar irradiance reported by Karalis (1989). The correlation between  $R_{s,368}$  and  $R_{d,368}$  was 0.82. The  $D_{368}$  had a slightly higher correlation ( $-0.85$ ) with PPFD than  $R_{d,368}$ . The correlation of  $\Delta$  with all other variables was less than 0.15. As expected, the aerosol transmittance was inversely correlated with  $D_{368}$  ( $-0.80$ ) and directly correlated with  $R_{s,368}$  (0.68).

#### a. Unlimited model

An unlimited stepwise regression on the measured PPFD considering terms  $R_{s,368}$ ,  $\Theta$ ,  $D_{368}$ ,  $\Delta$ ,  $\tau$ , and  $D_{368}^2$  resulted in

$$\text{PPFD} = 173 + 2105R_{s,368} - 101\tau + 60.7\Delta - 1.18\Theta + 668D_{368} - 764D_{368}^2, \quad (4)$$

where  $\Theta$  is in degrees. The model had an rmse of  $79 \mu\text{mol m}^{-2} \text{s}^{-1}$  and a coefficient of determination ( $r^2$ ) of

0.98 ( $F = 140\,594$ ,  $p = <0.0001$ ). This model, referred to later as the “unlimited model” provided the lower bound for expected errors in estimating the PPFD since no variable was explicitly excluded. Given the mean PPFD of  $932 \mu\text{mol m}^{-2} \text{s}^{-1}$  for all five locations, the rmse was equivalent to 8.5%; within the estimated  $\pm 13\%$  instrumentation error. The model rmse was higher than the approximate 5% rmse of the model developed by Alados and Alados-Arboledas (1999a,b). The contributions of  $\Theta$ ,  $\Delta$ ,  $\tau$ , and  $R_{d,368}$  in accounting for PPFD variability in the unlimited model were less than 0.01.

Similar consideration of unlimited stepwise regression on the measured PPFD for each location separately resulted in different models with lower rmse values than the all-location model described in Eq. (4) (Table 2) and percentage errors ranging from 4.4% to 7.8%. The rmse of the individual models was inversely proportional to the mean PPFD ( $r = 0.93$ ). Since cloud cover reduces PPFD, this inverse relationship may be evidence that cloud cover influenced the rmse values of the individual locations as well as the combined dataset. The probability of having clear skies, ideal for accurate model estimates of PPFD, varied from 8% to 18% across the study locations (Warren et al. 1986). These are lower probabilities of clear sky conditions than the 26% probability of clear skies in southern Spain (Warren et al. 1986) where Alados and Alados-Arboledas (1999a,b) developed and tested their models and may explain the higher rmse of the Eq. (4) model compared to the Alados and Alados-Arboledas models.

Although the unlimited models differed between locations, the dominant terms in these unlimited models were similar, with  $R_{s,368}$  and  $D_{368}^2$  contributing most to the PPFD model for Colorado ( $r^2 = 0.99$ ), New York ( $r^2 = 0.99$ ), and Utah ( $r^2 = 0.99$ ) and  $R_{s,368}$  and  $\Theta$  contributing most to the PPFD model for Mississippi ( $r^2 = 0.99$ ) and Indiana ( $r^2 = 0.99$ ). These two combinations of variables,  $R_{s,368}$  and  $\Theta$ , and  $R_{s,368}$  and  $D_{368}^2$ , were then used to describe the PPFD variability at all locations. Of the over 4000 linear and nonlinear models for these two combinations of variables explored using TABLECURVE, two variable-limited models were developed according to the previously described criteria.

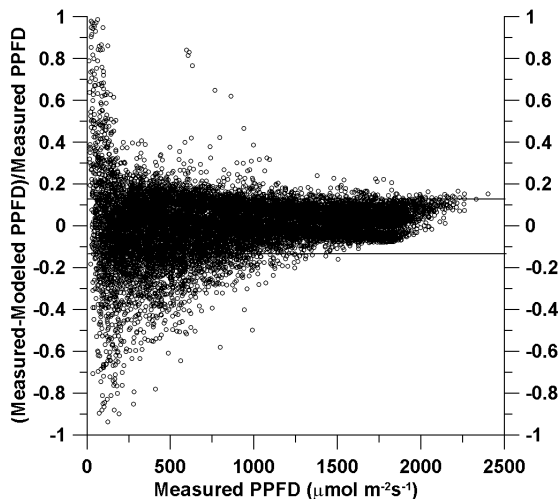


FIG. 2. Residual analysis for all locations of the model based only on global 368-nm measurements and solar zenith angle (model 1). The solid lines define the  $\pm 13\%$  instrumentation error bounds.

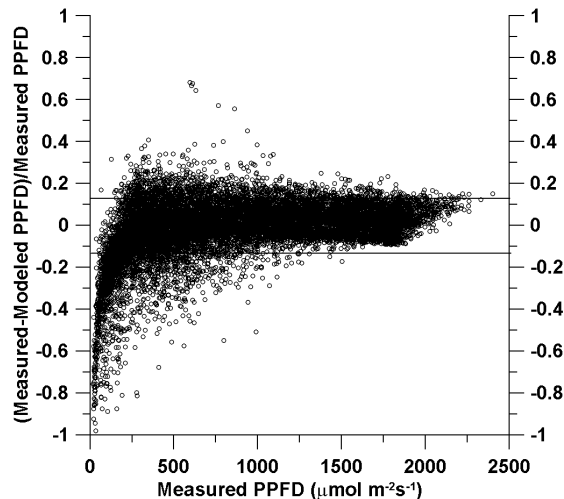


FIG. 3. Residual analysis for all locations of the model based on both global and diffuse 368-nm measurements (model 2). The solid lines define the  $\pm 13\%$  instrumentation error bounds.

### b. Variable-limited models

The first variable-limited model (model 1) estimated PPFD from  $R_{s,368}$  measurements and  $\Theta$ . The model rmse ranged from 52 to 72  $\mu\text{mol m}^{-2} \text{s}^{-1}$  for the five individual locations (Table 2). For all locations combined, the equation that best described the measured 3-min mean PPFD was

$$\text{PPFD} = -161 + 2822R_{s,368} - 329R_{s,368}^2 + 1.89\Theta. \quad (5)$$

The model accounted for 98% of the PPFD variability and had an rmse of 88  $\mu\text{mol m}^{-2} \text{s}^{-1}$  ( $r^2 = 0.98$ ,  $F = 238\,158$ ,  $p < 0.0001$ ). The rmse of this model, which included only two of the six terms of the unlimited model, was 9.4%, corresponding to 10  $\mu\text{mol m}^{-2} \text{s}^{-1}$  more error than the unlimited model. Sixty-three percent of the modeled values were within the  $\pm 13\%$  cumulative instrumentation error (Fig. 2). The model overestimated the PPFD under low PPFD more frequently than under high PPFD. The increased variability in the relative error of the model at PPFD less than 250  $\mu\text{mol m}^{-2} \text{s}^{-1}$  was most likely a result of statistical fluctuations associated with ratios of small values. Overestimates of the model under low PPFD were in part due to differences in the cosine response of the PAR sensor and the corrected response of the UV-MFRSR sensor. While relative errors were greater for PPFD less than 500  $\mu\text{mol m}^{-2} \text{s}^{-1}$ , the rmse for PPFD less than 250  $\mu\text{mol m}^{-2} \text{s}^{-1}$  was 36  $\mu\text{mol m}^{-2} \text{s}^{-1}$  while the mean bias error (MBE) was  $-5 \mu\text{mol m}^{-2} \text{s}^{-1}$  for a total error of 36  $\mu\text{mol m}^{-2} \text{s}^{-1}$ . This model resulted in a comparable estimate of PPFD to that of Karalis (1989), who estimated PAR (0.4–0.695  $\mu\text{m}$ ) based on global SW (0.3–3.0)  $\mu\text{m}$  with an rmse of 30  $\text{W m}^{-2}$  (approximately 140  $\mu\text{mol m}^{-2} \text{s}^{-1}$ ).

Modeling the PPFD at each individual location based

on the same variables resulted in rmse values ranging from 52  $\mu\text{mol m}^{-2} \text{s}^{-1}$  to 71  $\mu\text{mol m}^{-2} \text{s}^{-1}$  (Table 2) corresponding to a 5.4%–8.4% error. The rmse was inversely correlated with mean PPFD ( $r = 0.66$ ). The individual location rmse values were not correlated to mean AOD.

The second variable-limited model (model 2) estimated PPFD from the measured two components of the 368-nm channel of the UV-MFRSR: the global and diffuse component. For individual locations, the model rmse was between 55 and 69  $\mu\text{mol m}^{-2} \text{s}^{-1}$  (Table 2). For all locations combined, the equation that best described the measured 3-min mean PPFD was

$$\text{PPFD} = 191 + 2240R_{s,368} - 174D_{368}^2. \quad (6)$$

This model accounted for 98% of the variability in PPFD ( $r^2 = 0.98$ ,  $F = 383\,548$ ,  $p < 0.0001$ ). The model rmse was 85  $\mu\text{mol m}^{-2} \text{s}^{-1}$ ; up to 54% larger than the smallest rmse for individual locations and 23% larger than the locations with the greatest rmse. The rmse represented 9.1% of the mean PPFD. The model overestimated low PPFD (Fig. 3). This overestimate may be due to variable optical thicknesses of overcast skies and in part due to differences in the cosine response of the PAR sensor and the corrected response of the UV-MFRSR sensor. Sixty-four percent of the modeled values were within the  $\pm 13\%$  cumulative instrumentation error. Low irradiance conditions had greater relative error than high irradiance conditions but a smaller absolute error. For PPFD less than 250  $\mu\text{mol m}^{-2} \text{s}^{-1}$ , the total error of the model was 32  $\mu\text{mol m}^{-2} \text{s}^{-1}$  (rmse = 23  $\mu\text{mol m}^{-2} \text{s}^{-1}$ , MBE =  $-22 \mu\text{mol m}^{-2} \text{s}^{-1}$ ).

Modeling the PPFD at each individual location using the same variables resulted in rmse values ranging from 55  $\mu\text{mol m}^{-2} \text{s}^{-1}$  to 69  $\mu\text{mol m}^{-2} \text{s}^{-1}$  (Table 2) cor-

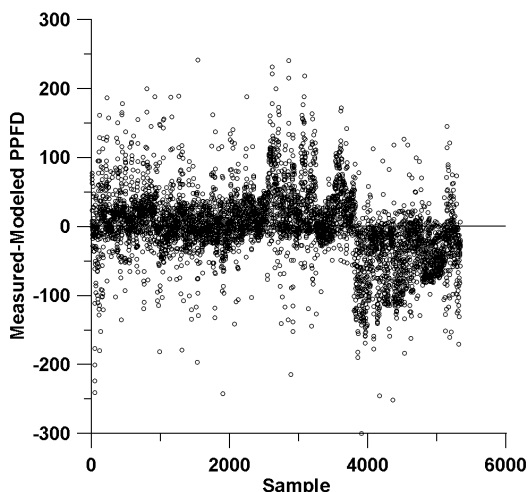


FIG. 4. Temporal variability in the model 1 residuals for the UT measurement location. Note the shift in model error near sample 4000.

responding to a 5.1%–7.5% error. The individual location rmse values of this model were correlated to mean PPFD ( $R = 0.81$ ) but not correlated to mean AOD.

#### c. Model error analysis

A comparison of the residuals of the two models shows the first model to have a more symmetrical residual, with a greater fraction of the modeled values falling within the measurement error. The residuals of model 1 were more symmetrical about zero at low PPFD than the second model (Figs. 2, 3). Regardless of the model developed, the locations at Utah, New York, and Colorado exhibited an unusual shift in the PPFD model error (Fig. 4). This shift resulted in a split in the model error with increasing PPFD, as illustrated in Fig. 1. It was determined that this shift did not coincide with 1) a UV-MFRSR sensor head change (Table 1), 2) a UV-MFRSR board change, or 3) a PPFD sensor change (Table 1). A study of the temporal variation in the 368 nm channel voltage intercepts of daily Langley plots for each 368-nm channel UV-MFRSR head (Slusser et al. 2000) showed no corresponding shift that would account for the evident shift in measured–modeled PPFD. As a result, we assumed that the shift was not produced by sensor failure or calibration correction errors. Consequently, all of the data were deemed valid and model errors include this shift effect.

There was an apparent impact of this shift on the rmse model errors. The location specific models 1 [Eq. (5)] and 2 [Eq. (6)] for these three locations were 8–10  $\mu\text{mol m}^{-2} \text{s}^{-1}$  higher than that of the unaffected Indiana and Mississippi location models (Table 2). Consequently, the inclusion of all the data probably did impact the overall model accuracy.

The biological significance of an error of 30  $\mu\text{mol m}^{-2} \text{s}^{-1}$  at low PPFD and 80  $\mu\text{mol m}^{-2} \text{s}^{-1}$  across all PPFD can be assessed by considering the impact that a

hypothetical accumulated error in the same direction (+ or –) throughout the day would have on crop productivity. The hypothetical accumulated error for one day from the 80  $\mu\text{mol m}^{-2} \text{s}^{-1}$  error corresponds to  $\pm 5 \text{ g CO}_2$  fixed  $\text{m}^{-2} \text{ day}^{-1}$  based on measurements of a maize canopy (Norman and Arkebauer 1991). The corresponding error at low PPFD levels would be approximately  $\pm 1.9 \text{ g CO}_2$  fixed  $\text{m}^{-2} \text{ day}^{-1}$  by the maize canopy. Assuming conversion of 0.68 g glucose per g  $\text{CO}_2$  fixed and 1.49 g glucose per gram of dry matter (DM) according to Vertregt and Penning De Vries (1987), the overall error in estimated PPFD can result in under- or overestimates of dry matter production in the maize canopy of 1.6 g DM  $\text{m}^{-2} \text{ day}^{-1}$ . This represents approximately 6% of a typical maize canopy assimilation rate of 29 g DM  $\text{m}^{-2} \text{ day}^{-1}$  (Norman and Arkebauer 1991).

#### 4. Conclusions

The best model to estimate the PPFD from the 368-nm channel irradiance measurements made by the UV-MFRSR instrument in the USDA UV-B Climate Monitoring Network depends on the availability of ancillary measurements. The best model included global and diffuse 368-nm irradiance, solar zenith angle, sky brightness, and aerosol transmittance and had a residual error of 79  $\mu\text{mol m}^{-2} \text{s}^{-1}$  PPFD. Aerosol transmittance is, however, difficult to determine under cloudy conditions. The best two-variable model (model 2), using the global and diffuse 368-nm irradiance, was slightly better than that using the global 368-nm irradiance and the solar zenith angle (model 1) with a residual error of 85  $\mu\text{mol m}^{-2} \text{s}^{-1}$  and a corresponding error of 32  $\mu\text{mol m}^{-2} \text{s}^{-1}$  for PPFD less than 250  $\mu\text{mol m}^{-2} \text{s}^{-1}$ .

The PPFD measurement error ( $\pm 5\%$ ) in combination with the UV-MFRSR measurement error ( $\pm 8\%$ ) was comparable to the 9% rms error for either two-variable model. Errors of the order of 80  $\mu\text{mol m}^{-2} \text{s}^{-1}$ , found for all models reported here, represent biologically significant amounts of dry matter production in crops such as maize. This indicates that, if possible, PPFD measurements should be made and not modeled.

*Acknowledgments.* Thanks go to Gwen Scott at the USDA UVB Monitoring and Research Office at Colorado State University for her extensive data manipulation in preparation for this analysis.

#### REFERENCES

- Alados, I., and L. Alados-Arboledas, 1999a: Direct and diffuse photosynthetically active radiation: Measurements and modeling. *Agric. For. Meteorol.*, **93**, 27–38.
- , and —, 1999b: Validation of an empirical model for photosynthetically active radiation. *Int. J. Climatol.*, **19**, 1145–1152.
- , I. Foyo-Moreno, and L. Alados-Arboledas, 1996: Photosynthetically active radiation: Measurements and modeling. *Agric. For. Meteorol.*, **78**, 121–131.

- Bigelow, D. S., and J. R. Slusser, 2000: Establishing the stability of multi-filter UV rotating shadowband radiometers. *J. Geophys. Res.*, **105**, 4833–4840.
- , —, A. F. Beaubien, and J. H. Gibson, 1998: The USDA ultraviolet radiation monitoring program. *Bull. Amer. Meteor. Soc.*, **79**, 601–615.
- Blackburn, W. L., and J. T. A. Proctor, 1983: Estimating photosynthetically active radiation from measured solar radiation. *Sol. Energy*, **31**, 233–234.
- Caldwell, M. M., C. L. Ballaré, J. F. Bornman, S. D. Flint, L. O. Börn, A. H. Teramura, G. Kulandaivelu, and M. Tevini, 2003: Terrestrial ecosystems, increased solar ultraviolet radiation and interactions with other climatic change factors. *Photochem. Photobiol. J.*, **2**, 29–38.
- Cen, Y.-P., and J. F. Bornman, 1990: The response of bean plants to UV-B radiation under different irradiances of background visible light. *J. Exp. Bot.*, **41**, 1489–1495.
- Flint, S. D., and M. M. Caldwell, 2003: A biological spectral weighting function for ozone depletion research with higher plants. *Physiol. Plantarum*, **117**, 137–144.
- González, L., and J. Calbó, 2002: Modelled and measured ratio of PAR to global radiation under cloudless skies. *Agric. For. Meteorol.*, **110**, 319–325.
- Grant, R. H., and W. Gao, 2003: Diffuse fraction of UV radiation under partly cloudy skies as defined by the Automated Surface Observation System (ASOS). *J. Geophys. Res.*, **108**, 4046, doi: 10.1029/2002JD002201.
- Grobner, J., M. Blumthaler, and W. Ambach, 1996: Experimental investigation of spectral global irradiance measurement errors due to a non-ideal cosine response. *Geophys. Res. Lett.*, **23**, 2493–2496.
- Gueymard, C., 1989a: An atmospheric transmittance model for the clear sky beam, diffuse and global photosynthetically active radiation. *Agric. For. Meteorol.*, **45**, 215–229.
- , 1989b: A two-band model for the calculation of clear sky solar irradiance, illuminance, and photosynthetically active radiation at the Earth's surface. *Sol. Energy*, **43**, 253–265.
- Harrison, L., and J. Michalsky, 1994: Objective algorithms for the retrieval of optical depths from ground-based measurements. *Appl. Opt.*, **33**, 5126–5132.
- , —, and J. Berndt, 1994: Automated multi-filter rotating shadowband radiometer: An instrument for optical depth and radiation measurements. *Appl. Opt.*, **33**, 5118–5125.
- Howell, T. A., D. W. Meek, and J. L. Hatfield, 1983: Relationship of photosynthetically active radiation to shortwave radiation in the San Joaquin Valley. *Agric. Meteorol.*, **28**, 157–175.
- Jakovidis, C. P., F. Timbros, D. N. Asimakopoulos, and M. D. Steven, 1997: Urban aerosol and clear skies spectra for global and diffuse photosynthetically active radiation. *Agric. For. Meteorol.*, **87**, 91–104.
- , —, —, K. M. Theofilou, and S. Pashiardes, 2003: Global photosynthetically active radiation and its relationship with global solar radiation in the eastern Mediterranean basin. *Theor. Appl. Climatol.*, **74**, 227–233.
- Karalis, J. D., 1989: Characteristics of direct photosynthetically active radiation. *Agric. For. Meteorol.*, **48**, 225–234.
- LiCOR, Inc., 1986: LI-COR terrestrial radiation sensors, type SB instruction manual. LiCOR, Inc. Publ. 8609-58, 25 pp.
- McCartney, H. A., 1978: Spectral distribution of solar radiation. II. Global and diffuse. *Quart. J. Roy. Meteor. Soc.*, **104B**, 187–208.
- McCree, K. J., 1966: A solarimeter for measuring photosynthetically active radiation. *Agric. Meteorol.*, **3**, 353–366.
- Norman, J. M., and T. J. Arkebauer, 1991: Predicting canopy photosynthesis and light use efficiency from leaf characteristics. *Modeling Crop Photosynthesis—From Biochemistry to Canopy*, K. J. Boote, and R. S. Loomis, Eds., CSSA Special Publication, Vol. 19, American Society of Agronomy and Crop Science Society of America, 75–94.
- Olsen, J. A., and A. Skartvelt, 1993: Luminous efficacy models and their application for calculation of photosynthetically-active radiation. *Sol. Energy*, **52**, 391–399.
- Papaoannou, G., N. Papanikolaou, and D. Retails, 1993: Relationships of photosynthetically active radiation and shortwave irradiance. *Theor. Appl. Climatol.*, **48**, 23–27.
- Rao, C. R. N., 1984: Photosynthetically active components of global solar radiation: Measurements and model computations. *Arch. Meteor. Geophys. Bioklimatol.*, **26**, 1–10.
- Scheirer, R., and A. Macke, 2001: On the accuracy of the independent column approximation in calculating the downward fluxes in the UVA, UVB, and PAR spectral ranges. *J. Geophys. Res.*, **106**, 14 301–14 312.
- Slusser, J. R., J. H. Gibson, D. S. Bigelow, D. Kolinski, P. Disterhoft, K. Lantz, and A. Beaubien, 2000: Langley method of calibrating UV filter radiometers. *J. Geophys. Res.*, **105**, 4841–4849.
- Spitters, C. J. T., H. A. J. M. Toussaint, and J. Goudriaan, 1986: Separating the diffuse and direct component of global radiation and its implications for modeling canopy photosynthesis. Part I. Components of incoming radiation. *Agric. For. Meteorol.*, **38**, 217–229.
- Taylor, R. M., A. K. Tobin, and C. M. Bray, 1997: DNA damage and repair in plants. *Plant and UV-B: Responses to Environmental Change*, P. Lumsden, Ed., Society for Experimental Biology Seminar Series, Vol. 64, Cambridge University Press, 53–76.
- Vass, I., E. Turcsányi, E. Touloupakis, D. Ghanotakis, and V. Petrouleas, 2002: The mechanism of UV-A radiation-induced inhibition of photosystem II electron transport studied by EPR and chlorophyll fluorescence. *Biochemistry*, **41**, 10 200–10 208.
- Vertregt, N., and F. W. T. Penning de Vries, 1987: A rapid method for determining the efficiency of biosynthesis of plant biomass. *J. Theor. Biol.*, **128**, 109–119.
- Warren, S. G., C. J. Hahn, J. London, R. M. Chervin, and R. L. Jenne, 1986: Global distribution of total cloud cover and cloud type amounts over land. NCAR Tech. Note NCAR/TN-273+STR, 229 pp.
- Zepp, R. G., T. V. Callaghan, and D. J. Erickson III, 2003: Interactive effects of ozone depletion and climate change on biogeochemical cycles. *Photochem. Photobiol. J.*, **2**, 51–61.